

## Albedo as a modulator of climate response to tropical deforestation

Paul A. Dirmeyer and J. Shukla

Center for Ocean-Land-Atmosphere Studies, Calverton, Maryland

**Abstract.** An atmospheric general circulation model with land surface properties represented by the simplified Simple Biosphere model is used to investigate the effects on local climate due to tropical deforestation for the Amazon basin. One control and three anomaly integrations of 4 years' duration are performed. In the anomaly integrations, rain forest in South America is replaced by degraded grassland. The anomaly integrations differ only in the optical properties of the grassland vegetation, with net surface albedos ranging from the same as to 0.09 lighter than that of rain forest. It is found that the change in climate, particularly rainfall, is strongly dependent on the change in surface albedo that accompanies deforestation. Replacement of forest by grass causes a reduction in transpiration and reduces frictional convergence by decreasing surface roughness. However, precipitation averaged over the deforested area is not necessarily reduced. Average precipitation decreases when the increase in albedo is greater than 0.03. If surface albedo is not increased appreciably as a result of deforestation, moisture flux convergence driven by the increase in surface temperature can offset the other effects, and average precipitation increases. As albedo is increased, surface temperature does not change, but surface latent and sensible heat flux decreases due to reduced radiational energy absorbed at the surface, resulting in a reduction in convection and precipitation. A change in the distribution of precipitation due to deforestation that appears to be independent of the albedo is observed.

### 1. Introduction

Changes at the land surface, whether natural or caused by human activity, can affect climate. The land is a source of and sink for heat and moisture for the atmosphere. Energy is exchanged between the surface and the air radiatively at visible and infrared wavelengths, through contact, or latently, through evapotranspiration. Evapotranspiration, whether transpiration from vegetation or direct evaporation from exposed surfaces, supplies moisture and heat to the atmosphere. In addition, momentum is transferred between the earth and the atmosphere via friction. These fluxes at the lower boundary act as forcings which help determine the state of the atmosphere locally and the circulation both locally and globally. Any changes in the soil or the vegetation that alter the fluxes of heat, moisture, or momentum will affect the atmospheric circulation [Dirmeyer and Shukla, 1993].

Climate change caused by changes in vegetation has received considerable attention recently. Of particular concern are vegetation changes of anthropogenic origin, particularly large-scale degradation brought about by poor land management. In such situations, entire biomes are destroyed and replaced by simpler biological communities. Examples include tropical deforestation for the harvesting of hardwoods or clearing for agriculture, desertification in semiarid regions caused by overfarming or overgrazing, and midlatitude deforestation by timber or agricultural interests. In each case, the amount of biomass is greatly reduced, surface

roughness and reflectivity change, and the amount of plant transpiration is diminished.

With atmospheric general circulation models (GCMs) coupled to biosphere models such as the Simple Biosphere (SiB) model of Sellers *et al.* [1986] or the biosphere atmosphere transfer scheme of Dickinson *et al.* [1986], the effects on climate of large-scale changes in vegetation can be studied by replacing or redistributing the biomes within the biosphere model. There have been many modeling studies of Amazon deforestation [e.g., Henderson-Sellers and Gornitz, 1984; Dickinson and Henderson-Sellers, 1988; Lean and Warrilow, 1989; Nobre *et al.*, 1991; Dickinson and Kennedy, 1992; Henderson-Sellers *et al.*, 1993; Polcher and Laval, 1993; hereinafter referred to as HSG, DHS, LW, NSS, DK, HS, and PL, respectively]. Of these, all but DHS show reductions in rainfall between 0.5 and 1.8 mm d<sup>-1</sup>. In such studies, deforestation is simulated by replacing the rainforest biome by a degraded pasture biome with much shorter roughness length and reduced ability to transpire moisture. Net surface albedos are increased 0.05 to 0.10 in these experiments. Garratt [1993] and HS present reviews of the principal deforestation studies; the former also compares the various land surface schemes used.

Dirmeyer [1992] found in both short integrations over the Amazon and multiyear integrations of cases with idealized topography that the prescribed albedo change may be critical in determining the response of climate to tropical deforestation. Experiments with a flat rectangular continent centered on the equator showed that precipitation anomalies were negative when deforestation was accompanied by an increase in albedo and positive when albedo did not increase as a result of deforestation. The circulation anomalies were

Copyright 1994 by the American Geophysical Union.

Paper number 94JD01311.  
0148-0227/94/94JD-01311\$05.00

also very dependent on albedo. The Amazon integrations showed similar effects but were of 1 year's duration or less and thus of questionable significance. This study is motivated by those previous findings; we intend to validate those results with longer integrations using realistic terrain and boundary conditions.

We know that albedo changes directly affect the surface energy balance. In semiarid regions, an increase in albedo leads to a loss of radiative energy absorbed at the surface, and convective overturning is reduced [Charney *et al.*, 1977; Chervin, 1979]. As a result, precipitation decreases. Evaporation may also decrease, further inhibiting precipitation [Sud and Fennessy, 1982; Laval and Picon, 1986; Sud and Molod, 1988]. However, the drying effects are not limited to the subtropics. Similar reductions in precipitation and evapotranspiration have been found for increased albedo in tropical Africa [Kitoh *et al.*, 1988] and the Amazon basin [Mylne and Rowntree, 1992].

There is reason to believe that smaller albedo changes than those proposed in the experiments by DHS, LW, NSS, HS, and PL may be more realistic. For example, the optical properties of the degraded grassland in the report by NSS were chosen to be identical to those of temperate grasses. However, Stephens and Greenwald [1991] show that clear sky components of the Earth Radiation Budget Experiment data and Nimbus 7 data over grassland areas of the North American Great Plains give net surface albedos that appear to be no more than 0.06 higher than those over the Amazon. Recent in situ measurements by Bastable *et al.* [1993] indicate that noontime albedos over Amazon forest were  $0.128 \pm 0.005$ , while values over deforested clearings were  $0.157 \pm 0.008$ . Mean daily values also differed by only about 0.03 on average. Measurements at other deforested field sites show average increases in albedo of about 0.05–0.06 (C. Nobre, personal communication, 1992).

There will always be some uncertainty in predicting the true albedo of a largely deforested Amazon. Soil types vary across the region, as does the vegetation that replaces the forest. These variations contribute to fluctuations in net surface albedo. There are also variations in time. Typically, when an area is cleared by burning, a great deal of ash is contributed to the soil. This ash helps to keep soil albedos low. The land is usually put into use for farming for a few years and then converted to grazing land as the nutrient-poor soil is depleted. These grasslands are often recleared periodically by burning, adding more ash to the soil. Burning can drastically reduce surface albedo on the seasonal timescale [Fisch *et al.*, 1994] and reduce the long-term surface albedo by the continued presence of dark ash (P. Sellers, personal communication, 1993). Some areas are neglected after clearing and revert to a type of degraded forest with thick ground cover. Albedos for all such vegetation types vary.

The uncertainties in the specification of albedo may have major implications for the surface energy balance of the region, which could affect the response of local climate to deforestation. Deforestation with large increases in albedo has been shown to cause significant decreases in evapotranspiration and rainfall in the modeling experiments of LW, NSS, and HS. LW find that large reductions in moisture flux convergence are primarily a result of the albedo increase. However, the same effects may not occur when albedo increases are small. One would expect smaller albedo increases to allow more energy to be available at the surface

for heating the lower atmosphere. Possible results include a smaller curtailment of evapotranspiration and greater low-level convergence. These effects could prevent a large drop in rainfall. Therefore this study seeks to address how the degree of change in albedo associated with deforestation affects the response of local climate. Several experiments are conducted and compared with the results of previously published experiments, especially those of NSS.

Section 2 describes the GCM and vegetation model used. The framework of the deforestation experiments is explained in section 3. Section 4 presents results, including a diagnosis of the interannual variability with which the response must be compared. Section 5 presents a synthesis of the results, outlining a general schematic for the response of the general circulation to tropical deforestation. Results from previous studies and experiments with idealized topography are used to help determine a composite response. Conclusions are summarized in section 6.

## 2. Description of the Model

In all experiments, the Center for Ocean-Land-Atmosphere Studies (COLA) atmospheric general circulation model is used with specified lower boundary conditions over ocean and a biosphere model over land. The atmospheric general circulation model used is a research version of the National Meteorological Center global spectral model described by Sela [1980] with modifications and boundary conditions as described by Kinter *et al.* [1988]. The model is discretized into 18 vertical layers, with resolution concentrated near the lower boundary. The model is integrated for 4 years with a rhomboidal truncation at total wavenumber 15. This translates to a grid resolution of approximately  $7.5^\circ$  of longitude by  $4.5^\circ$  of latitude. A Gaussian grid is used by the model for all physics calculations.

The radiative processes in the GCM include the diurnally varying radiation scheme of Harshvardhan *et al.* [1987], the shortwave transfer scheme described by Lacis and Hansen [1974] as modified by Davies [1982], and the longwave scheme of Harshvardhan and Corsetti [1984]. Boundary layer fluxes are those used in the E2-Physics package of the Geophysical Fluid Dynamics Laboratory model by Miyakoda and Sirutis [1986]. Vertical diffusion in the boundary layer is based on the second-order closure model of Mellor and Yamada [1982]. Convection and large-scale precipitation are computed by a modification of the scheme of Kuo [1965] as described by Sela [1980], and the shallow convection scheme is that of Tiedke [1984]. The GCM uses the interactive model-generated cloud scheme of Hou [1990].

The lower boundary conditions for the GCM are supplied as follows. The biosphere model used to provide boundary conditions over land is a simplified version of the Simple Biosphere (SiB) model of Sellers *et al.* [1986], which is described by Xue *et al.* [1991], and is referred to hereafter as SSiB. Initial soil moisture and temperature are computed by using the soil moisture data of Willmott *et al.* [1985] and the soil temperature method of Delsol *et al.* [1971]. The integrations have seasonally varying climatological sea surface temperatures [Slutz *et al.*, 1985].

There are significant differences between this experiment and that of NSS. The current version of the GCM has the interactive model-generated cloud scheme of Hou [1990], whereas in that of NSS clouds were specified as a function of

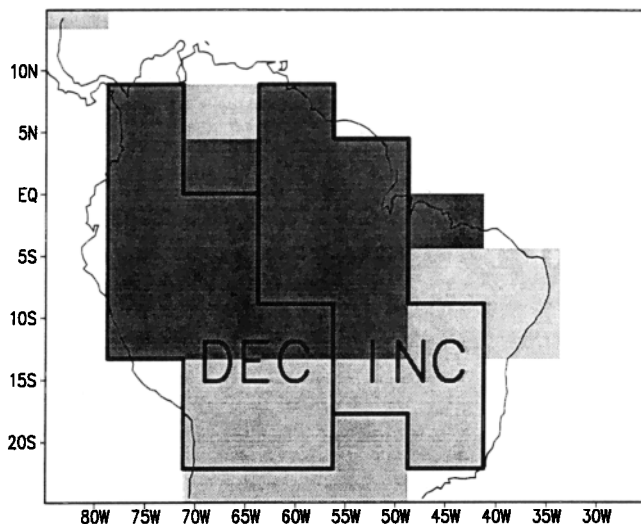


**Figure 1.** Model representation of northern South America. The shaded area denotes land points. Dark shading covers the area (deforested, DEF) which is rainforest in the control case and degraded grass in the anomaly cases. Outlined areas DEC and INC correspond to regions where rainfall tends to decrease and increase, respectively, and are used in moisture budget calculations.

latitude and time of year. The seasonally varying sea surface temperatures (SSTs) are in contrast to those of NSS, who held SSTs at December values throughout the integration. In addition, the specification of the "degraded grassland" vegetation in the deforested region is slightly different from that of NSS because of the change from SiB to SSiB. The main point of this study is that here, several different albedos are used in the various deforestation integrations.

### 3. Description of Experiments

The investigation of Amazon deforestation is conducted with the use of the medium-resolution (R15) GCM with realistic topography. The R40 version of the GCM produces a more realistic climatology but is prohibitively expensive to integrate for the amount of time needed to produce statistically meaningful results for all experiments. The control integration is started from observed conditions at 0000 UTC September 1, 1990, and integrated for 3 months to reduce the effect of the initial conditions. From the resulting 0000 UTC December 1, 1990, conditions, three deforested integrations are initialized. Both control and deforested integrations are carried out for 4 years from that point.

In all three deforested integrations, the SSiB rainforest vegetation type is replaced by degraded grassland over South America. Figure 1 shows the grid points where the vegetation type is changed. The only difference between the three cases is the specification of albedo in the deforested area. Table 1 shows the reflectances and net surface albedos for control and deforested cases. Changes are made to canopy and soil albedos in both visible and near-infrared wavelengths to achieve the given net changes. In deforested case D0, the annual average surface albedo over degraded grass is the same as over the rainforest of the control (CTL) case. The albedo in the other two deforested cases, D6 and D9, is increased by 0.06 and 0.09, respectively. The 0.09 value corresponds to the increase used by NSS, and the 0.06 value is near the typical measured value discussed earlier and is also halfway between the low measured value of *Bastable et al.* [1993] and that of NSS.

In the control case, the values for key vegetation parameters used in SSiB are as follows. Canopy height is taken to be 35 m, and the roughness length is 2.65 m. The displacement height is 27.4 m. It is assumed that there is 98% coverage of the surface by vegetation and that the leaf area index is about 5.0. The depth to which roots penetrate the soil (and thus the depth of the reservoir of moisture available for transpiration) is 1.5 m. For all of the deforested cases, the canopy height is 0.6 m. Roughness length averages about 0.076 m, and displacement height is about 0.25 m, although these quantities do vary slightly with the seasons. Similarly, leaf area index varies between 1.15 and 2.15 during the year. There is 80% coverage of the ground by vegetation, and the rooting depth is 1 m.

## 4. Results

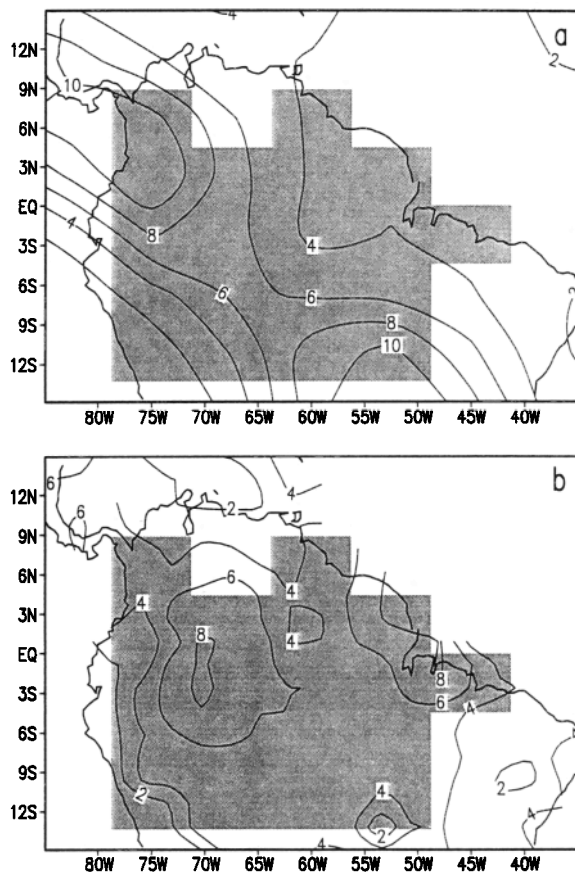
### 4.1. Moisture and Energy

Figure 2 shows the distribution of precipitation in the CTL averaged over 48 months. Observed annual mean precipitation, derived from station data compiled by the Climate Analysis Center (CAC) Climate Anomaly Monitoring System for the period 1979–1992 is also shown. The simulated rainfall rates over the Amazon basin and their distribution are reasonable. The model overpredicts the band of precipitation over the southeast. Other data sets of observed precipitation [e.g., *Figueroa and Nobre, 1990*] indicate greater mean rainfall rates to the southeast of the Amazon basin than shown in Figure 2b, but there is nonetheless excessive precipitation over this region in the model. The shortcomings in the simulation may be due to the effect of low resolution, as these precipitation features are better simulated in the R40 version of the model.

**Table 1.** Optical Properties of the Vegetation in the Control and Deforested Cases

Case	Reflectance						Net Surface Albedo
	Live Vegetation		Dead Vegetation		Soil		
	Visible	Near IR	Visible	Near IR	Visible	Near IR	
Control	0.100	0.450	0.160	0.390	0.110	0.225	0.134
D0	0.105	0.450	0.160	0.390	0.070	0.140	0.134
D6	0.105	0.577	0.360	0.577	0.110	0.225	0.191
D9	0.130	0.640	0.460	0.640	0.110	0.225	0.220

IR, infrared.



**Figure 2.** (a) The 48-month mean precipitation for the control case and (b) mean observed rainfall for 1979–1992. Units, millimeters per day. Shading, rainforest area.

The anomalies in precipitation for each deforestation case are shown in Figure 3. All cases show the same basic pattern: a pair of dipoles with minima to the east and maxima to the west. The dipole in the north represents a weakening of the climatological rainfall maximum, with a broadening of the high rainfall rates along the intertropical convergence zone (ITCZ) toward the western Atlantic. The southern dipole flanks the southern precipitation maximum, indicating a shift of the feature to the east.

There is a clear modulation of this basic pattern as a function of albedo. The anomalies in D0 show a broad, strong band of increased rainfall near the Atlantic coast and a weaker band of reduced rainfall parallel to and inland from the first band. Rainfall rates increase by more than 20% in the area between the Orinoco and Amazon Rivers. In D6, the positive anomaly band is weaker and more broken than in D0. The area of negative anomalies is stronger, particularly in the north. In D9, the case with the greatest change in albedo, the area of negative anomalies is very broad and strong, with decreases of more than 20% over a wide area. The area of positive anomalies is actually stronger than that in D6 but is shifted to the east of the position in the other deforested cases.

The areas of increased and decreased precipitation are very robust between cases, although there is some shifting of the dividing line toward the east as the albedo over the deforested area increases. Nonetheless, we may define two

geographically fixed areas, called DEC and INC, which roughly correspond to the regions of negative and positive anomalies, respectively. These are shown in Figure 1, in addition to the area of actual deforestation (DEF). The average precipitation anomalies computed over INC, DEC, and DEF are shown in Figure 4 as a function of change in net surface albedo over DEF. There is a clear trend in each area toward decreasing precipitation as albedo increases.

The change in time-mean evapotranspiration (ET) in response to deforestation is quite similar in all three cases (Figure 5). There is a general decrease in ET over all but the northwest portion of the deforested area, but nowhere does the anomaly exceed  $1 \text{ mm d}^{-1}$ . The magnitude of the anomaly is generally  $0.2\text{--}0.4 \text{ mm d}^{-1}$ . There is some variation in the magnitude of the anomalies between cases, but it is not clearly a systematic response to albedo. Decreases in ET are generally less than 15% in the north, with isolated decreases of 15–25% in the south.

The relatively weak response of ET to deforestation suggests that changes in ET are not directly causing the precipitation anomalies. Table 2 shows the terms of the

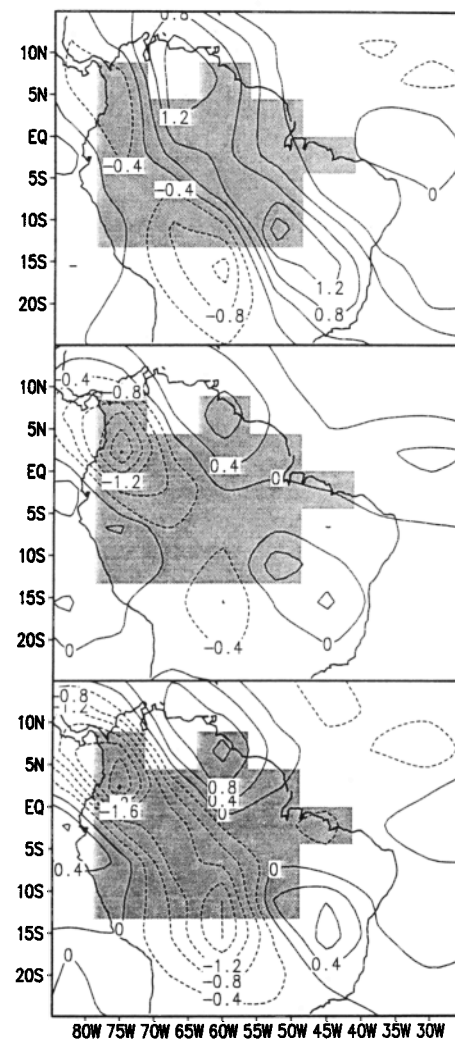


**Figure 3.** The 48-month mean precipitation anomalies for the deforested cases: (top) D0 – CTL, (middle) D6 – CTL, and (bottom) D9 – CTL. Contour interval is  $0.4 \text{ mm d}^{-1}$ . Shading denotes area of deforestation.

surface moisture balance over the deforested area. ET drops about 7% as a result of the change in vegetation and decreases further, as much as 12%, when the albedo increases. However, precipitation increases in the case of deforestation with no net albedo change and then drops steadily as albedo increases. Changes in precipitation most strongly mirror changes in the vertically integrated moisture flux convergence (MFC).

As shown previously, changes are not uniform over the area. Table 3 shows the terms of the hydrological balance for land and atmosphere computed separately over INC and DEC for each case. Anomalies in ET are again small and over INC are of the opposite sign of changes in precipitation. The systematic trends in MFC are quite clear. As albedo increases, moisture flux convergence decreases in both areas. Positive anomalies in MFC become smaller over INC, and negative anomalies become larger over DEC. Changes in runoff mirror changes in precipitation, with a tendency to offset the reductions in ET. All cases show a positive change in soil moisture (computed as a residual) during the 4-year period. It has been found that the initial soil moisture used [Willmott *et al.*, 1985] is not in equilibrium with the model over much of northern South America. By comparison of the time series for year 1 with other years, the time scale for adjustment is deduced to be 3–6 months, with an increase in soil wetness of at most 0.13.

The pattern of anomalies of MFC (not shown) looks very much like that of the precipitation anomalies. The dynamical supply of moisture in the atmosphere has changed because the general circulation has changed in response to the deforestation. It appears that the physical changes that occur as a result of deforestation cause a robust change in regional flow that shifts the distribution of moisture flux convergence and rainfall. This shift is modulated by the degree of albedo change associated with the deforestation.

The terms of the surface energy balance over the area of deforestation are given in Table 4. Latent heat flux from the surface decreases somewhat as a result of the change in vegetation and falls further in response to increasing albedo. This was shown previously for ET and is consistent with the finding of other modeling studies of Amazon deforestation by LW, NSS, HS, and PL. Also consistent with those studies are the increase in upward net longwave radiation

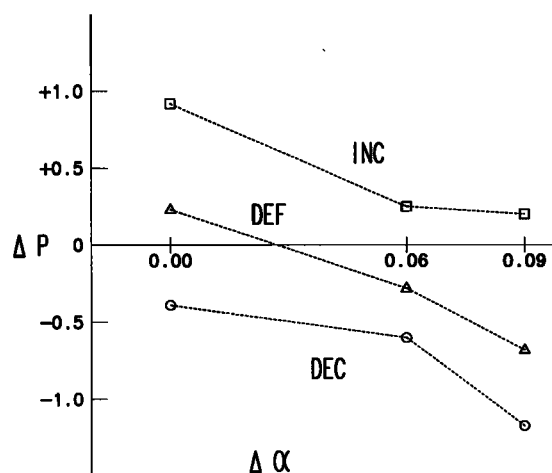


Figure 4. Time mean change in precipitation rate as a function of albedo change in each area DEF, DEC, and INC.

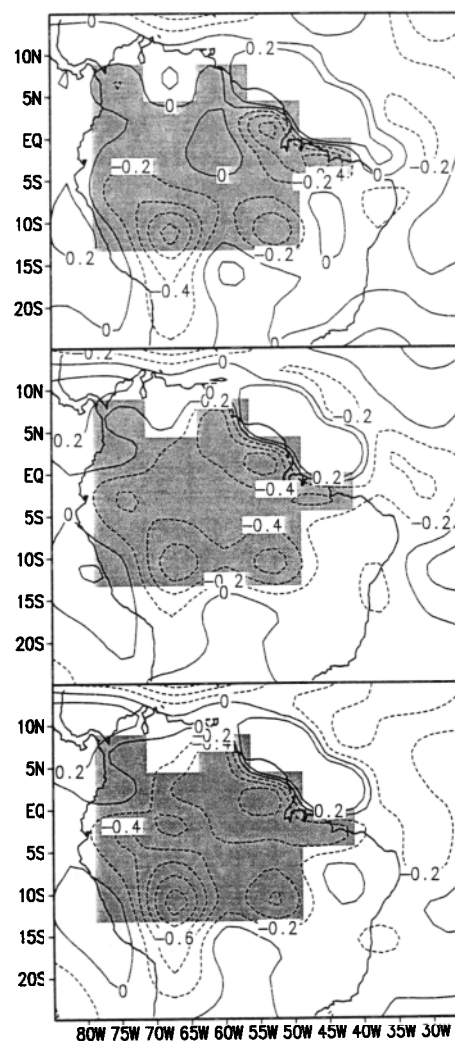


Figure 5. The 48-month mean evapotranspiration anomalies for the deforested cases: (top) D0 – CTL, (middle) D6 – CTL, and (bottom) D9 – CTL. Contour interval is 0.2 mm  $d^{-1}$ . Shading denotes area of deforestation.

and surface temperature and the decrease in the sum of the fluxes of latent and sensible heat. A reduction in cloud cover is also documented by DK and PL.

There are, however, elements of the surface energy balance which are different from previous results. In the current experiment, sensible heat flux does not increase as a result of deforestation. This is true even though the surface temperature increases by 2 K and may be due to the large reduction in roughness. The magnitude of the decrease grows as the

Table 2. Time Mean (48 Months) Surface Moisture Budget Over DEF

	Control	D0	D6	D9
P	5.94	6.17	5.66	5.26
ET	3.21	3.00	2.88	2.83
MFC	2.73	3.17	2.78	2.43
Runoff	2.70	3.10	2.71	2.37

Units are millimeters per day. P, precipitation; ET, evapotranspiration; MFC, moisture flux convergence.

**Table 3.** Time Mean (48 Months) Surface Moisture Budget Over Areas of Northern South America

	Control		D0		D6		D9	
	DEC	INC	DEC	INC	DEC	INC	DEC	INC
P	6.10	6.51	5.56	7.43	5.52	6.76	4.94	6.71
ET	2.95	3.18	2.71	3.04	2.73	2.85	2.64	2.85
MFC	3.15	3.33	2.85	4.39	2.79	3.91	2.30	3.86
Runoff	3.11	3.24	2.77	4.29	2.70	3.81	2.21	3.79

Units are millimeters per day. DEC, area of decreased rainfall; INC, area of increased rainfall. Other abbreviations are as in Table 2.

albedo increases, but sensible heat flux decreases slightly even when there is no change in albedo. Another related difference is the lack of change in the Bowen ratio between cases. The time-mean fluxes of latent and sensible heat tend to vary proportionally.

Some interesting effects of albedo on the surface moisture and energy balances are revealed. Precipitation actually increases over the deforested area in response to the change in vegetation with no albedo increase, even though ET decreases. The same is also true of moisture flux convergence, where the increase as a result of the change in vegetation is even greater. As the albedo of the degraded grassland rises, precipitation and moisture flux convergence diminish. These effects have also been seen in experiments with idealized topography and in simulations of Amazon deforestation at higher resolution [Dirmeyer, 1992]. We also find that the increase in downward shortwave flux at the ground is largely a function of albedo and its effect on cloudiness. The difference in surface shortwave radiation between cases D0 and CTL is small. On the other hand, the increase in net longwave radiation is strictly a result of the change in vegetation and its effect on surface temperature. This is in contrast to the findings of DK, who state that roughness changes systematically affect the difference between net longwave radiation and shortwave absorbed at the surface. One might expect changes in precipitation to vary directly with cloud cover and inversely with changes in downward shortwave at the surface. As can be seen from Tables 2 and 4, this is not entirely the case. The apparent inconsistencies are a manifestation of a change in the nature of the convection and will be described later in concurrence with the diurnal cycle.

#### 4.2. Seasonal Cycle

The annual cycle of precipitation is compared with the 1979–1992 mean observed annual cycle, compiled from the CAC Climate Anomaly Monitoring System data (supplied to COLA by J. E. Janowiak). Figure 6 compares the seasonal cycles within each area. Subject to possible sampling problems in using data for sparsely distributed stations, there is

good agreement between the simulation and observations for most times. However, the amplitude of the annual cycle in the model is generally too large. This is caused by an excess of GCM rainfall in the local wet season, particularly over the two maxima in precipitation shown in Figure 2. This effect is averaged out over the DEF area. The phase of the seasonal cycle is reasonable in all three areas. The peaks of the rainy seasons tend to be shifted slightly, but the timing of the dry seasons is quite good. Both DEC and DEF show a secondary peak in September. This is the result of the model ITCZ returning southward much sooner than observed. Also, convective precipitation in the south is generally too strong and too far south during the southern rainy season. Both shortcomings may be due to the relatively low spatial resolution of the model. Precipitation in this integration is generally weak over the western tropical Atlantic and strong over land. These problems were not seen in the 1-year integration at R40 [Dirmeyer, 1992].

Deforestation introduces an anomaly in precipitation whose shape and phase are very similar for all three anomaly cases. Differences between cases take the form of variations in the amplitude of the anomalies and the annual means. Figure 7 shows the anomalies in the seasonal cycle of precipitation over each area. Over the DEF area, there is a tendency for the wet season to arrive and end sooner than in the control case. May through July are drier in each of the deforested cases, and January is wetter. The changes in other months are not systematic. D0 tends toward more rainfall than the control case (8 months of the year) and always more than the other deforested cases. D9 has the least precipitation in 9 of the 12 months. In the INC area, the amplitude of the seasonal cycle of rainfall is increased. There is a tendency in each case for the rainy season to be wetter and the dry season drier. In the DEC area, the rainy season is much drier in every deforested case. The rainy season also ends more abruptly, although the onset is not affected. Most of the variation between cases occurs during the dry season and the secondary wet season late in the year.

In each area, the change in ET has a similar pattern (not

**Table 4.** Time Mean (48 Months) Surface Energy Budget, Cloud Cover, and Surface Temperature Over a Deforested Area

	Control	D0	D6	D9
Latent heat	93	87	83	82
Sensible heat	54	51	48	46
Net longwave	34	45	46	46
Shortwave down	-213	-216	-224	-229
Shortwave up	29	29	43	50
Cloud cover	0.73	0.71	0.69	0.68
Surface temperature	297	299	299	299

All fluxes are positive upward (in watts per square meter). Units of temperature are degrees Kelvin. Cloud cover is dimensionless.

shown). During the rainy season, there is little difference between the control and deforested cases. In the D0 case, ET actually increases during this period as more energy is absorbed by the dark soil and vegetation. During the dry seasons, monthly mean ET rates drop by as much as  $0.9 \text{ mm d}^{-1}$ . The drying of the partially exposed soil surface and the grassland's lack of available soil moisture (due to shallower rooting depth) and transpiration capacity combine to reduce moisture flux from the ground.

Figure 8 shows the seasonal cycle of the terms of the moisture balance for the deforested area in each case. In the control case, MFC dominates over ET during the wet season of March–May. ET is lowest during this time and is highest during the dry season. The maximum rate of depletion of soil moisture occurs in August. In the deforested cases D0 and D6, MFC is greater than ET for 6 months of the year. The amplitude of the seasonal cycle of ET is much smaller in the deforested cases, as available soil moisture is depleted in June and July. In case D9, MFC declines like ET. The maximum depletion of soil moisture occurs during July in all deforested cases, corresponding to the earlier arrival of the month of least precipitation.

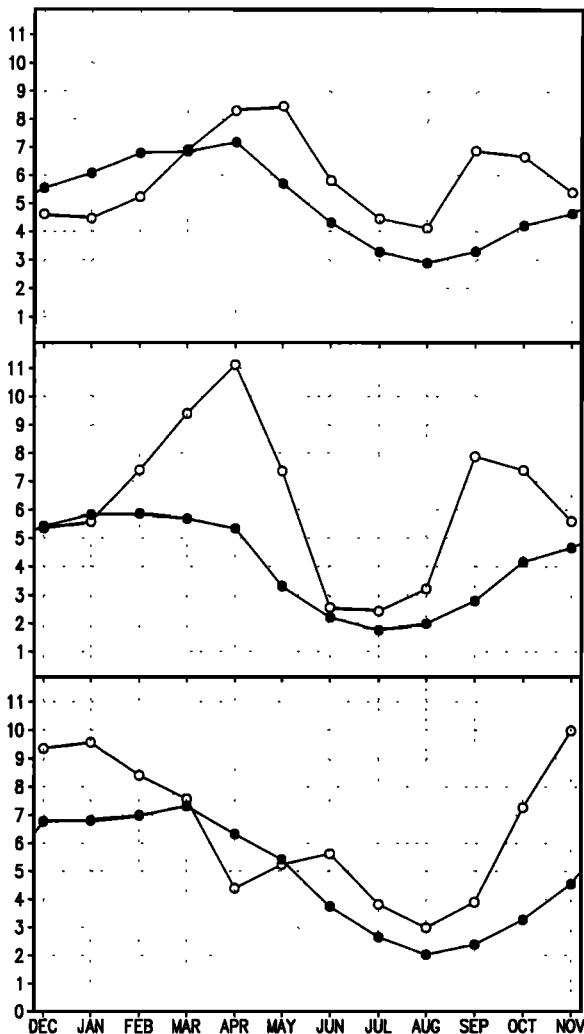


Figure 6. Mean annual cycle of precipitation for the control case (open circles) and station climatologies (solid circles) in the areas of (top) DEF, (middle) DEC, and (bottom) INC. Units are millimeters per day.

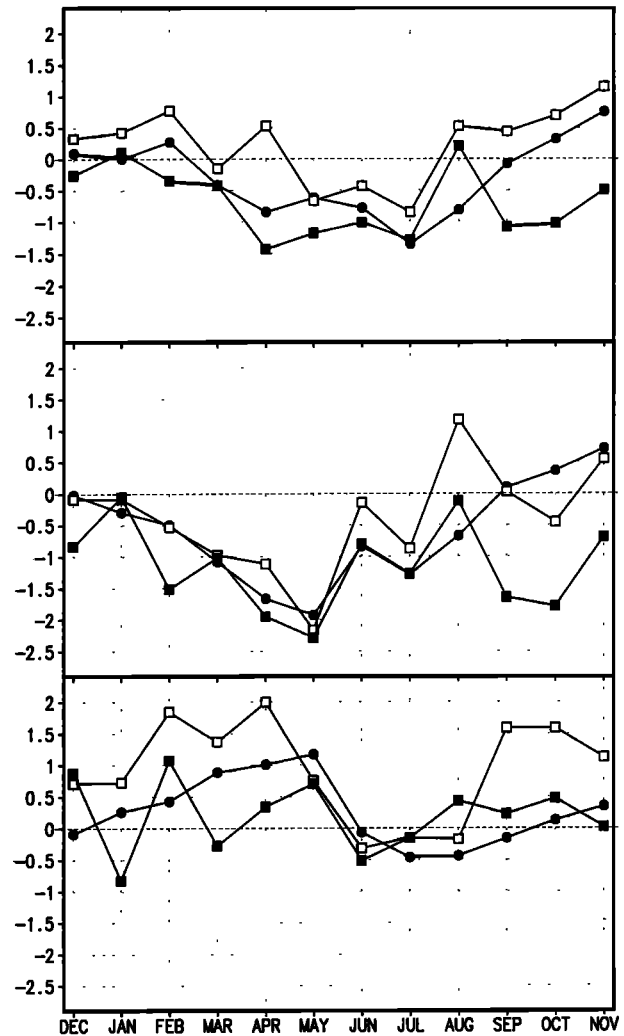


Figure 7. Mean annual cycle of precipitation change for each deforested case averaged over (top) DEF, (middle) DEC, and (bottom) INC. Open squares, D0 – CTL; solid circles, D6 – CTL; solid squares, D9 – CTL. Units are millimeters per day.

#### 4.3. Interannual Variability

Despite the facts that the SSTs are climatological and the seasonal cycle of vegetation is specified globally, there is considerable interannual variation in the model. Figure 9 shows the annual mean precipitation anomalies for D6 for each of the 4 years of integration compared with the 4-year mean for the CTL. Annual averages for D6 are shown because they show most clearly the variety of anomaly patterns. However, each integration has comparable variations. The interannual persistence of anomalies appears to be most robust in the northern Amazon. The area of reduced rainfall in the north is present in every year, although the magnitude varies by a factor of 3. The northern region of increased rainfall near the coast is evident in years 1, 3, and 4 but missing in year 2. The southern extrema that were so prominent in Figure 2 are less robust. The region of decreased rainfall in the south is clear in years 2 and 3 but only weakly present in year 1 and absent in year 4. The southern maximum is well defined only in year 2 and is displaced, distorted, or missing in other years. Annual anomalies for D9

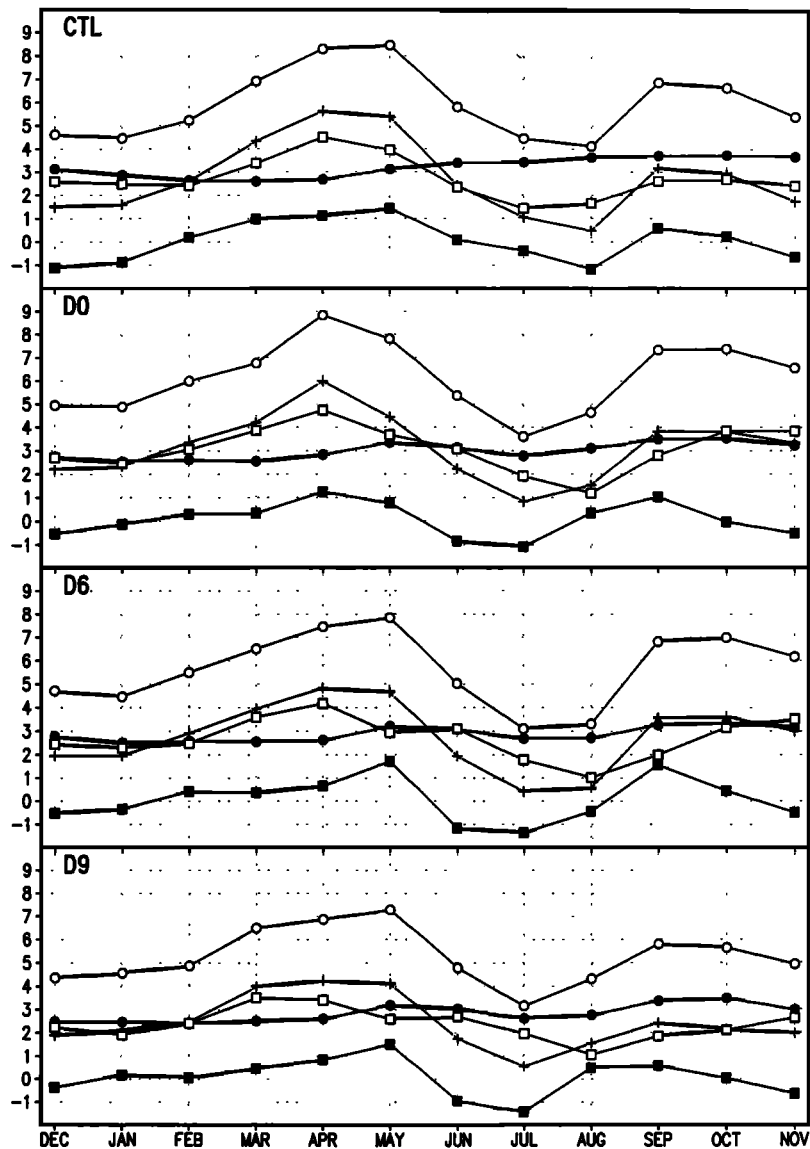


Figure 8. Mean annual cycle averaged over DEF of precipitation (open circles), evapotranspiration (solid circles), moisture flux convergence (pluses), runoff (open squares), and change in soil moisture computed as a residual (solid squares). Units are millimeters per day.

show more permanence of features, but the magnitudes of the extrema still vary from year to year.

The high degree of variation in rainfall over the Amazon raises concerns about the significance of the anomalies due to deforestation in the model. To verify that the magnitudes of the precipitation anomalies are significantly larger than the natural variability of the model, time series of the deforestation anomalies are compared with series of the variation in the control case about its own climatologies. Monthly means of precipitation are computed at each grid point for CTL and each deforested case for all 48 months. An annual cycle climatology for CTL is computed from the 4-year integration. We then compute the variance of the difference between CTL and its climatology and use it as a measure of natural variability. Similarly, variances of the difference between each of the deforested series and the CTL climatology are computed. The ratio of the variances is equivalent to the value of Fisher's  $F$  test of significance of

variances [Panofsky and Brier, 1958]. As shown in Table 5, the anomalies over the areas do significantly exceed the natural variability of the control case. It was found that the average lifetime of a precipitation anomaly (defined as the number of consecutive months that the mean monthly precipitation anomaly averaged over the area maintained the same sign) was not significantly different from what would be expected if monthly precipitation anomalies were determined by a random process. Therefore, a value of 1.61 is significant at the 95% level, and 1.96 is significant at 99%. The anomalies in each case were also found to be significant at 95% at almost all individual grid points over northern South America. Some grid points over the Nordeste region and near the southern climatological rainfall maximum were not significant at 95%.

We have also examined the interannual variability of monthly mean rainfall anomalies about a 4-year mean climatology for each case separately. This is equivalent to the



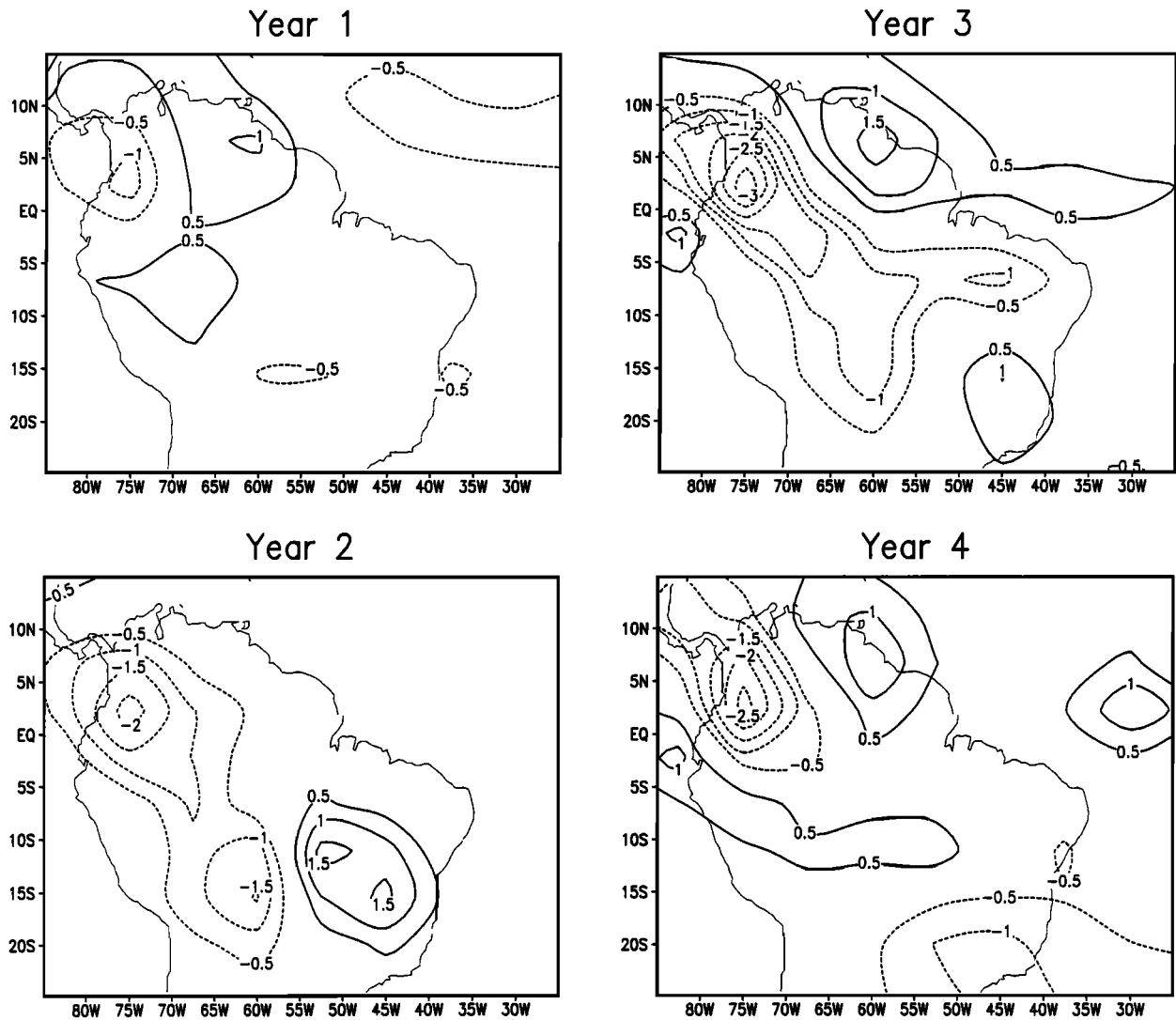


**Figure 9.** Mean anomalies in precipitation rate ( $D6 - CTL$ ) for each year of the integration. Contour interval is  $0.5 \text{ mm d}^{-1}$ ; zero contour is omitted.

internal variability of climate within each case. In the DEC area, the magnitude of the internal variability of each deforested case is diminished compared with that of the CTL. The same is true in the other two areas for D6 and D9. For D0, the internal variability increases compared with that of CTL in the areas DEF and INC. Table 6 illustrates this. Despite the differences between cases, similar spatial patterns exist in each case. Interannual variability increases in each deforested case along the Venezuelan and Colombian coasts and over Peru (not shown).

**Table 5.** Ratio of Variances of Monthly Precipitation Anomalies (Deforested Minus Control Climatology Divided by Control Minus Control Climatology)

Area	D0	D6	D9
DEF	2.68	2.35	2.25
DEC	2.35	2.35	2.31
INC	2.60	1.82	1.82

DEF, deforested; DEC, decreased rainfall; INC, increased rainfall. Values above 1.60 are significant at the 95% confidence level.

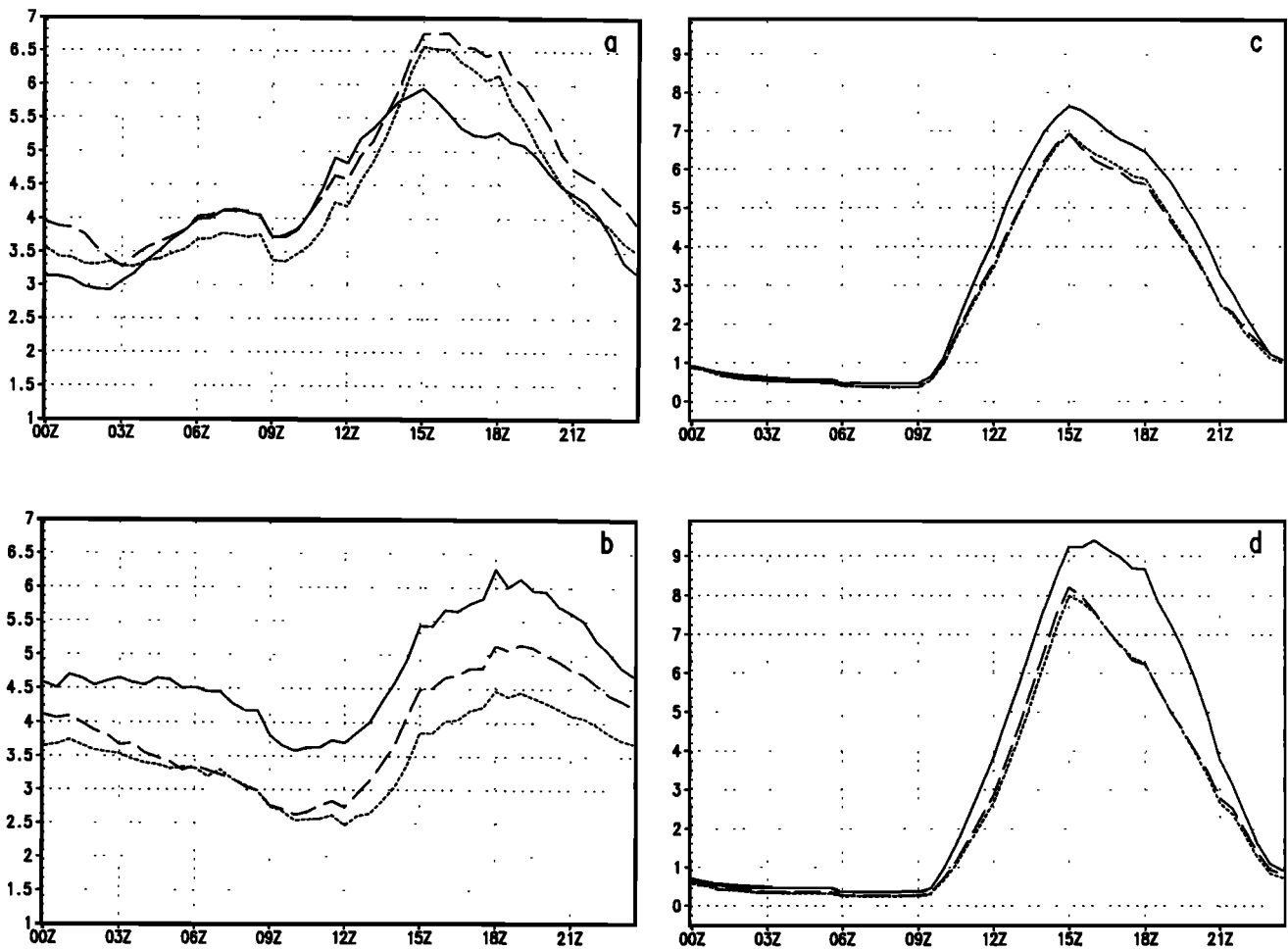
#### 4.4. Diurnal Cycle

Figure 10 shows the mean January and July diurnal cycles for precipitation, ET, and surface temperature over the deforested area. Only three cases are shown: control, D0, and D9. In January, precipitation in the deforested cases tends to be greater than in the control case in the afternoon and evening hours and less than or about the same as in the control overnight and during the morning. D0 rainfall is greater than that in the control during most of the day. In July, both deforested cases have consistently less rainfall than the control throughout the day. In both seasons, D0

**Table 6.** Monthly Variance of Precipitation Within Each Case About Its 4-year Mean Annual Cycle

Area	Control	D0	D6	D9
DEF	3.23	3.59	2.74	2.39
DEC	3.17	3.07	2.93	2.08
INC	3.45	4.02	2.57	2.49

Units Are ( $\text{mm}^2 \text{ d}^{-2}$ ).



**Figure 10.** Diurnal cycle averaged over DEF for CTL (solid line), D0 (dashed line), and D9 (dotted line). (a) January and (b) July precipitation, (c) January and (d) July evapotranspiration, and (e) January and (f) July surface temperature. Precipitation and evapotranspiration are in millimeters per day; temperature is in degrees Kelvin.

rainfall exceeds D9 rainfall at all times. This is generally true for INC and DEC as well as at individual grid points. The deforested area spans rainy and dry zones, so budgets over this area at any time average together the changes in the two regimes. Examination of smaller areas reveals that during the dry season, the amplitude of the diurnal cycle of rainfall is reduced. The afternoon maximum in precipitation is not as strong in the deforested cases. During the rainy season, however, there is no consistent response in the diurnal cycle to deforestation. There is either a systematic reduction at all hours or an amplification of the diurnal cycle prompted by an increase in afternoon convective precipitation.

Changes in ET are very similar for D0 and D9. Both show a reduction compared with the control case, especially after the midday peak. The diurnal cycle of ET over localities during the rainy season is unchanged from control to deforested cases. During the local dry season, ET over the grassland increases during the morning, much like over the forest. However, ET reaches its peak sooner and at a lower rate than over the forest and then drops abruptly. The result is a net reduction in daily mean ET of 50% at some grid points. The strong afternoon reduction over dry areas contributes to the skewness apparent in Figure 10d. Over regions of DEC outside the deforested area, where precipi-

tation drops due to deforestation but there is still an adequate supply of soil moisture, ET increases. The extra solar radiation available due to the decrease in cloudiness contributes to increased latent heat flux from the surface.

The amplitude of the diurnal cycle of surface temperature increases dramatically because of deforestation. The amplitude generally increases by a factor of 2. In some small regions, increases of greater than a factor of 3 are found. The increase is especially noticeable in rainy season areas, where the diurnal cycle of the control case is very weak. Afternoon temperatures are locally 3–10 K warmer, 7–8 K when averaged over the DEF area. In July, deforested surface temperatures are cooler during the morning and warmer during the afternoon and evening. In January, the deforested surface is warmer throughout the day.

## 5. Changes in the Circulation

We illustrate the changes to the tropical circulation during December, January, and February (DJF) and June, July, and August (JJA) by examining plots of the anomalies. These periods represent the maximum in seasonal differences in the general circulation in the tropics and the positions of the rain bands. In DJF, the southern Amazon basin is in the midst of

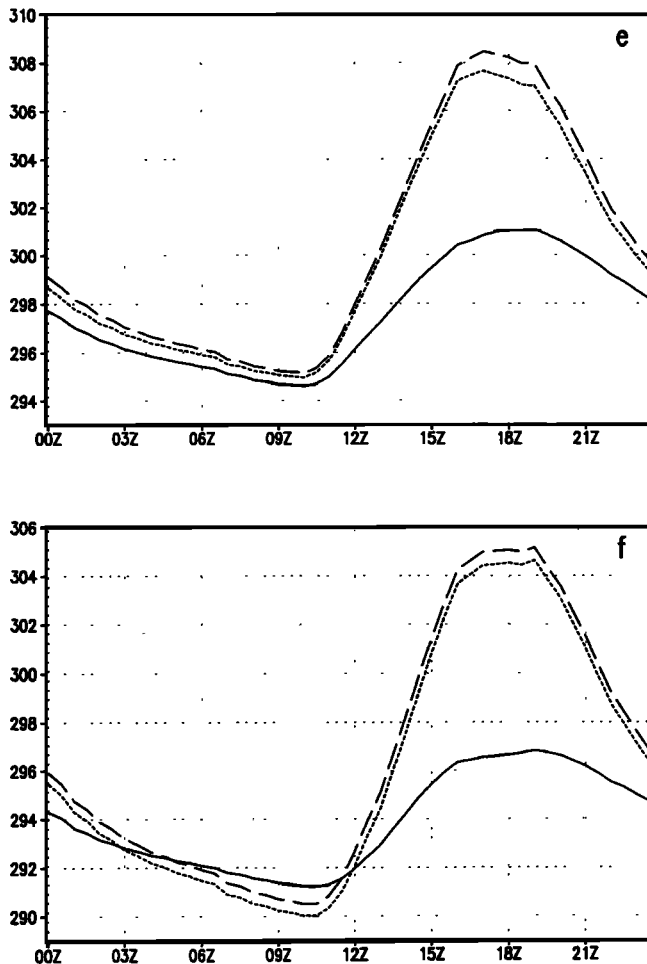


Figure 10. (continued)

the rainy season, and the north is dry; the opposite is true in JJA. In Figure 11, the vectors represent anomalies at the 850-hPa level. The vertical motion anomalies are at 500 hPa. Only anomalies are illustrated, not the total flow.

Figure 11a is a diagram of the DJF flow anomalies for the case of deforestation with large increase in albedo (D9 minus CTL). There is a large area of sinking centered over the southwestern margin of the Amazon basin. To its east along the coast is a band of increased lifting that extends into the South Atlantic. These two areas correspond to southern regions of suppressed and increased precipitation in Figure 3c. A weaker anomaly of rising motion extends northward and westward along the coast and includes all of South America north of the equator. DJF is the dry season over this northern area, and the mean vertical motion over land is usually downward during this time. As a result, the lifting anomaly causes little change in rainfall except over the eastern Pacific, where anomalous lifting strengthens precipitation in the ITCZ. There is also a weak subsidence anomaly off the Atlantic coast between  $10^{\circ}$  and  $15^{\circ}$ S. In the lower troposphere, there is anomalous onshore flow from the Atlantic Ocean over much of the Amazon basin. The easterly anomaly in the equatorial zone reaches a maximum over the center of the basin and rises over the Andes and the west coast, contributing to the anomalous lifting there. In the south, westerly anomalies exist. They are especially strong

between the dipole in vertical velocity. The anomalous low-level flow out of the region of subsidence helps feed the lifting along the coast. Between the equatorial easterlies and the subtropical westerlies lies an anomalous ridge. There is a weaker anomalous ridge in the northern hemisphere.

The DJF anomalies for deforestation with no albedo change (D0 minus CTL) are shown in Figure 11b. There is a great deal of similarity to Figure 11a, as both show the same principal vertical velocity features. However, there are many differences in the details. The southwestern subsidence region is weaker by about 40%. The ascending region to the north is stronger and is more connected in a band to the southeastern ascending region. The subsidence off the east coast has shifted to cover northeast Brazil. The low-level onshore flow is still strong off the Atlantic, but there is less flow traversing the Amazon and Andes to feed lifting over the eastern Pacific and more low-level convergence over the basin itself.

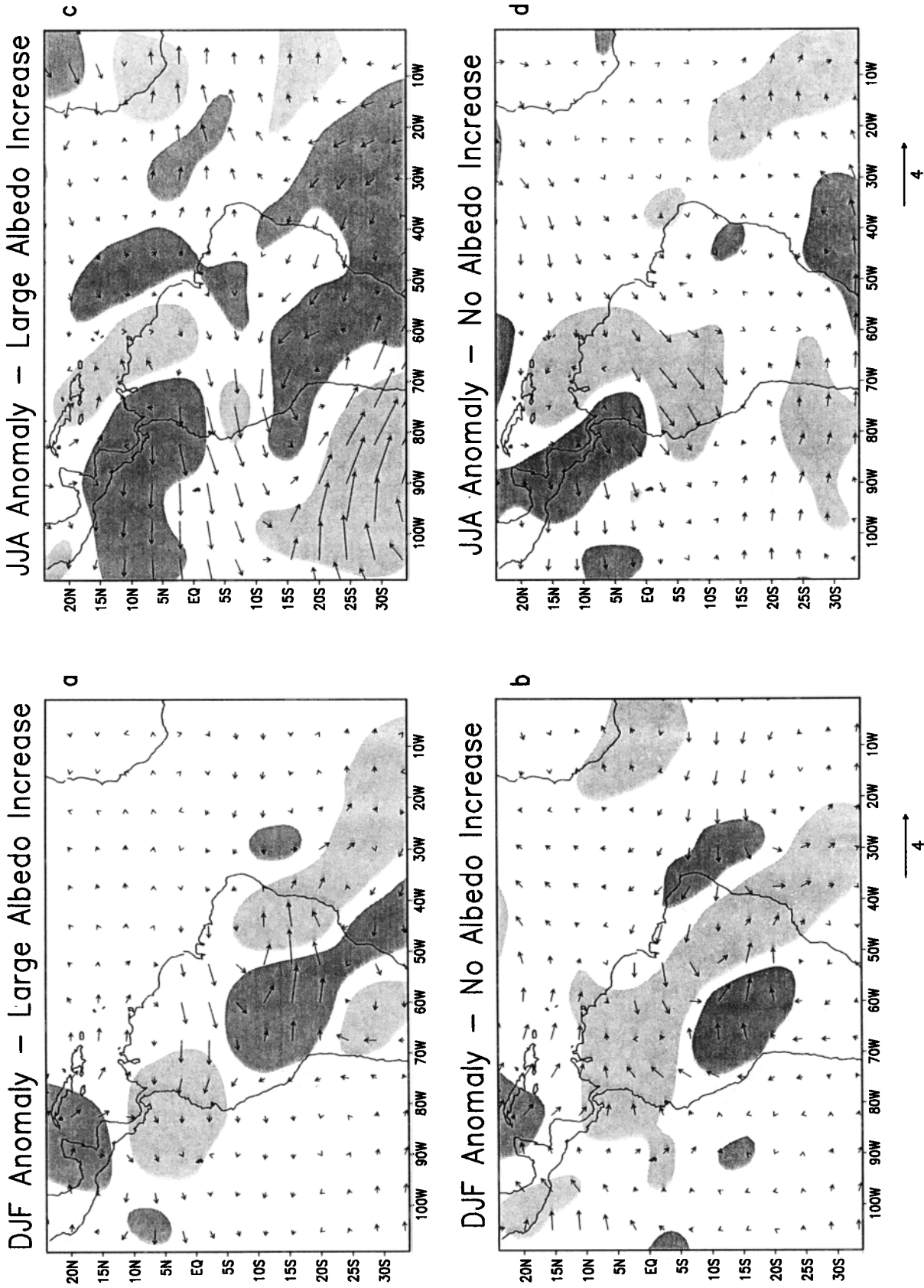
Figure 11c is a diagram of the JJA flow anomalies for D9 minus CTL. There are broad regions of subsidence over much of the southern Amazon and South America, the equatorial Atlantic, and off the southeast coast, accompanied by divergence at lower levels. In the equatorial band, there are low-level easterlies over western South America and the eastern Pacific and westerlies over the Atlantic. Poleward of  $10^{\circ}$  north and south, there is onshore flow from the Atlantic. There is strong sinking over Colombia and the eastern Pacific ITCZ, and there is an area of lifting over the northern Amazon east of  $70^{\circ}$ W.

Figure 11d shows the JJA anomalies for D0 minus CTL. The dominance of sinking motion seen over the area in the high-albedo case is now absent. However, subsidence over Colombia, Central America, and the eastern Pacific is still present. Low-level easterlies are also still present over western South America, but the pronounced westerlies over the tropical Atlantic are gone. There are two main areas of anomalous lifting: the northern Amazon (as in the high-albedo case) and a large area of the western and southwestern Amazon basin, where anomalous northeasterlies are forced upward orographically.

The annual mean 200-hPa circulation anomalies and 500-hPa vertical velocity anomalies for each case are shown in Figure 12. Westerly anomalies dominate in each case. The circulation for D9 (Figure 12a) indicates an anomalous trough over the southern Amazon basin, suggesting cooler tropospheric temperatures than the control case. This is consistent with reduced latent heat release accompanying reduced convection. There are upper-level ridges apparent in both hemispheres in the anomaly field of D0 (Figure 12b), suggesting accentuated heating in the lower and mid-troposphere. There is also clear indication of stronger outflow to the east of South America associated with the anomalous lifting.

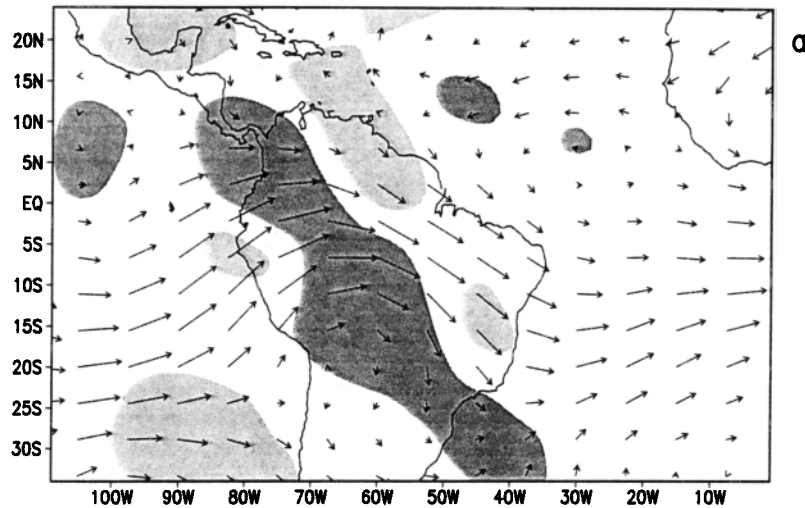
## 6. Discussion and Conclusions

It is instructive to synthesize the results by splitting the effects of deforestation into two categories: changes due to the change in vegetation alone, and changes due to albedo increase. First, a synopsis of the climate of the control case is in order. In the equatorial region over the Atlantic and South America, there is an easterly downgradient flow in the lower troposphere into the region of heating and low surface



**Figure 11.** Circulation anomalies due to deforestation for (a) large albedo increase (D9 - CTL), DJF; (b) no albedo increase (D0 - CTL), DJF; (c) large albedo increase (D9 - CTL), JJA; (d) no albedo increase (D0 - CTL), JJA. Arrows are wind anomalies at 850 hPa; scale vector (in meters per second) is at bottom. Light shading indicates areas of lifting anomalies (less than -4 mbar d<sup>-1</sup>), and dark shading shows areas of subsidence anomalies (>4 mbar d<sup>-1</sup>) at 500 hPa.

## Annual Anomaly – Large Albedo Increase



## Annual Anomaly – No Albedo Increase

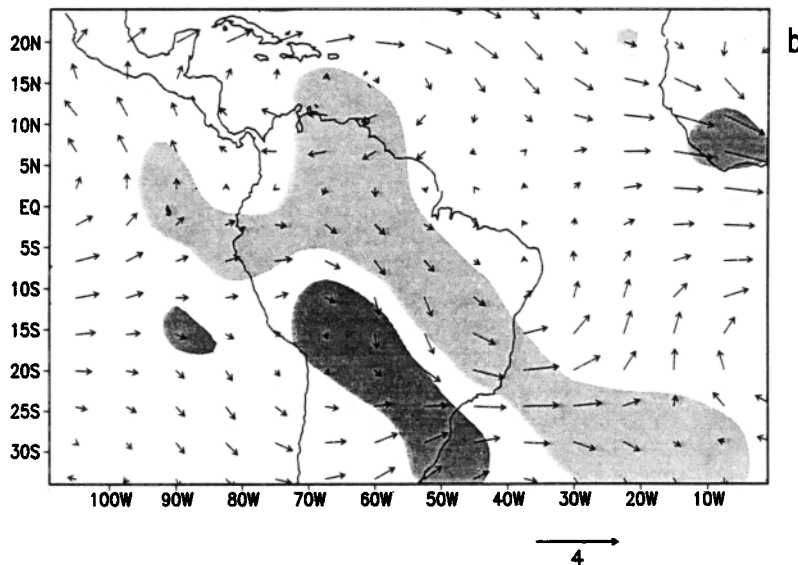


**Figure 12.** Annual mean circulation anomalies due to deforestation for (a) large albedo increase (D9 – CTL) and (b) no albedo increase (D0 – CTL). Arrows are wind anomalies at 200 hPa; scale vector (in meters per second) is at bottom. Light shading indicates areas of lifting anomalies (less than  $-4 \text{ mbar d}^{-1}$ ), and dark shading shows areas of subsidence anomalies ( $>4 \text{ mbar d}^{-1}$ ) at 500 hPa.

pressure over South America. The flow advects a great deal of moisture from the Atlantic over the Amazon basin. This tropical easterly flow is present throughout the year.

During the southern summer, a thermal cyclone forms over Bolivia, helping to induce a northerly component to the low-level flow over the southern Amazon basin. Also, the subtropical anticyclone over the southern Atlantic is a robust feature. Because of the shape of the Atlantic basin, which in the southern subtropics is longitudinally narrower and further east than in the northern subtropics, southward recurvature of the low-level flow over South America is also encouraged. Additionally, the ITCZ over the ocean stays north of the equator, so the southern branch of the Hadley circulation dominates the tropics over the eastern Atlantic. All these factors help to induce a monsoon-like pattern of

rain over subtropical South America during southern summer. The GCM overpredicts the magnitude of this summer maximum in precipitation. During southern winter the cyclone over Bolivia is replaced by a weak anticyclone, which prevents the northeasterly flow into the region of the southern annual rain maximum. Instead, most of the moisture is advected into the northern Amazon basin.

In each season, there is a great deal of moisture convergence into the foothills of the Andes. However, the precipitation is not wholly driven by the orography. The maxima in rainfall generally do not coincide with the maximum orographically induced lifting, suggesting the importance of thermally driven convergence in this area.

Next we consider the effect of the vegetation change in the model from rainforest to degraded grassland with no net

change in surface albedo. *Dirmeyer* [1992] has shown that low-albedo deforestation leads to opposite anomalies in transpiration versus evaporation from soil, particularly during the wet season. The change in vegetation leads directly to reduced transpiration, likely caused by decreases in leaf area (surface area where transpiration takes place) and plant moisture potential (rooting depth, density, and moisture availability). Reduction in the leaf area also reduces interception and re-evaporation of rainfall. The soil surface is more exposed to open air, and evaporation from the ground itself increases. However, this increase in direct evaporation is smaller than the decrease in transpiration, as the large reduction in roughness caused by the change in vegetation helps to impede evaporation. The net decrease in evapotranspiration is evident in Figure 5 and is relatively independent of albedo change. The reduction in roughness also suppresses the flux of sensible heat from the surface. This, combined with reduced evaporation, allows the surface temperature to rise, especially during the day. The increase in surface temperature boosts the net upward flux of longwave radiation. Since there is only a small change in the incoming shortwave, this increase in net longwave radiation offsets the reduced fluxes of sensible and latent heat, maintaining the surface energy balance (compare CTL and D0 in Table 4).

Dynamically, one might expect the decrease in roughness to reduce low-level convergence. However, the increase in thermally driven convergence caused by increased surface temperature offsets the reduction in frictional convergence. This helps transport and condense more moisture over the deforested area, adding another source of anomalous heating to further augment convergence. More tropical moisture is advected westward across the Atlantic coastline in the tropics, but the same amount is transported southward out of the region around the subtropical ridge. The recurvature occurs farther east, as the increase in surface temperature over the Amazon basin helps shift the center of the thermal low eastward. The result is that moisture convergence occurs further east as well, increasing rainfall along the coast and slightly decreasing it inland. In the north, a similar shift of the heating center away from the Andes shifts precipitation eastward. Rainfall in the Atlantic ITCZ and over the Caribbean decreases, as more moisture is drawn into South America.

Increasing net surface albedo in the model has a very different effect. A change in surface albedo manifests itself through radiational changes. Less shortwave radiation is absorbed at the surface, so less energy is available for sensible and latent heating. The surface temperature is only slightly cooler, since less heat is being removed by mechanical processes. However, the air temperature in the boundary layer is considerably cooler. Cloud cover is reduced as less energy and moisture are available for lifting and condensation. The reduction in cloudiness allows more shortwave radiation to reach the surface, partially offsetting the decrease in absorption and helping maintain higher surface temperatures. These effects combine to allow only a small increase in net upward longwave radiation, due primarily to increased absorption by the cooler boundary layer. The main anomaly balance, however, is between the decrease in shortwave absorbed and the decrease in surface heat fluxes (compare D0 and D9 in Table 4). The effect of increased

albedo is very much like that proposed by *Charney et al.* [1977] for the subtropics.

Reduced radiational heating of the atmospheric column (and increased cooling to space) leads to a subsidence anomaly. Thus the thermally driven convergence over the Amazon basin is reduced, and less moisture is pumped through the circulation. The reduction in convergence allows more moisture to advect westward from the basin out over the eastern Pacific. There is a general reduction in precipitation over the entire Amazon and an increase over adjacent waters of the Atlantic, Pacific, and Caribbean. Generally, the anomalies described above are most evident during the heat of the day, when fluxes of radiation, heat, and moisture are greatest. Also, anomalies in the surface energy terms tend to be largest during the local dry season, although changes in the general circulation affect both summer and winter hemispheres.

Currently, deforestation in the Amazon is patchy, with a great deal of variation at small scales. This heterogeneity might be expected to induce rather than retard convection by forming mesoscale circulations [*Pielke et al.*, 1991]. Eventually, assuming continued rates of destruction of rainforest, patchiness will give way to widespread clearing. *Eltahir and Bras* [1994] find decreases in precipitation of about 10% for deforestation of a patch 250 km on a side in a mesoscale model. This area is larger than observed patches but smaller than most GCM grid boxes. They assumed a net surface albedo increase of about 0.08. It is not clear from this experiment how albedo variations might affect the response to deforestation on small scales.

The results of this model study corroborate the findings of other deforestation studies for large increases in surface albedo. Nevertheless, given the paucity of field measurements, one can have little faith in current estimates of changes in albedo. Before the effects of deforestation can be forecasted, knowledge of albedo change is essential. Also, the degree to which sensitivity to albedo depends on the radiation and convective schemes used in various GCMs is not completely clear. The Kuo convective scheme used in our GCM has an inherently strong link between changes in precipitation and MFC. *Sud et al.* [1993] used the Goddard Laboratory for Atmospheres GCM with a different convective scheme [*Arakawa and Schubert*, 1974] and established that surface albedo changes have an impact in the tropics. Regardless, further testing with different models is needed to verify the separate dependencies of climate on albedo and vegetation change.

**Acknowledgments.** All figures were prepared using the Grid Analysis and Display System, and B. Doty provided much assistance in development and display of the graphics. This research was supported by National Science Foundation grant ATM-90-19296, with computational support from National Aeronautics and Space Administration grants NAGW-2661 and NAGW-1269. Additional computer time was provided by the NASA Center for Computational Studies.

## References

- Arakawa, A., and W. H. Schubert, Interaction of cumulus cloud ensemble with the large-scale environment, part I, *J. Atmos. Sci.*, 31, 674-701, 1974.
- Bastable, H. G., W. J. Shuttleworth, J. H. C. Gash, R. L. G. Dallarosa, G. Fisch, and C. A. Nobre, Observations of climate,

- albedo and surface radiation over cleared and undisturbed Amazonian forest, *J. Climatol.*, 13, 783–798, 1993.
- Charney, J. G., Dynamics of deserts and drought in the Sahel, *Q. J. R. Meteorol. Soc.*, 101, 193–202, 1975.
- Charney, J. G., W. J. Quirk, S. H. Chow, and J. Kornfield, A comparative study of the effects of albedo change on drought in semi-arid regions, *J. Atmos. Sci.*, 34, 1366–1385, 1977.
- Chervin, R. M., Response of the NCAR general circulation model to changed land surface albedo, in Report of the JOC Study Conference on Climate Models: Performance, Intercomparison and Sensitivity Studies, Washington, D. C., *GARP Publ. Series*, 22(1), 563–581, 1979.
- Davies, R., Documentation of the solar radiation parameterization in the GLAS Climate Model, *NASA Tech. Memo.*, TM-83961, 57 pp., 1982.
- Delsol, F., K. Miyakoda, and R. H. Clarke, Parameterized processes in the surface boundary layer of an atmospheric circulation model, *Q. J. R. Meteorol. Soc.*, 97, 181–208, 1971.
- Dickinson, R. E., and P. Kennedy, Impacts on regional climate of Amazon deforestation, *Geophys. Res. Lett.*, 19, 1947–1950, 1992.
- Dickinson, R. E., A. Henderson-Sellers, P. S. Kennedy, and M. F. Wilson, Biosphere-atmosphere transfer scheme (BATS) for the NCAR Community Climate Model, *Tech. Note TN-275TSTR*, Natl. Cent. for Atmos. Res., Boulder, Colo., 1986.
- Dirmeyer, P. A., GCM studies of the influence of vegetation on the general circulation, Ph.D. dissertation, 227 pp., Univ. of Md., College Park, 1992.
- Dirmeyer, P. A., and J. Shukla, Observational and modeling studies of the influence of soil moisture anomalies on the atmospheric circulation, in *Predictions of Interannual Climate Variations, NATO ASI Ser., Ser. I*, vol. 6, edited by J. Shukla, pp. 1–23, Springer-Verlag, New York, 1993.
- Eltahir, E. A. B., and R. L. Bras, Sensitivity of regional climate to deforestation in the Amazon basin, *Adv. Water Resour.*, in press, 1994.
- Figueroa, S. N., and C. A. Nobre, Precipitation distribution over central and western tropical South America, *Climanalise*, 5(6), 36–40, 1990.
- Fisch, G., J. R. Wright, and H. G. Bastable, Albedo of tropical grass: A case study of pre- and post-burning, *J. Climatol.*, 14, 103–118, 1994.
- Garratt, J. R., Sensitivity of climate simulations to land-surface and atmospheric boundary-layer treatments: A review, *J. Clim.*, 6, 419–449, 1993.
- Harshvardhan, and T. G. Corsetti, Longwave radiation parameterization for the UCLA/GLAS GCM, *NASA Tech. Memo.*, TM-86072, 65 pp., 1984.
- Harshvardhan, R. Davies, D. A. Randall, and T. G. Corsetti, A fast radiation parameterization for general circulation models, *J. Geophys. Res.*, 92, 1009–1016, 1987.
- Henderson-Sellers, A., and V. Gornitz, Possible climatic impacts of land cover transformations, with particular emphasis on tropical deforestation, *Clim. Change*, 6, 231–258, 1984.
- Henderson-Sellers, A., R. E. Dickinson, T. B. Durbridge, P. J. Kennedy, K. McGuffie, and A. J. Pitman, Tropical deforestation: Modeling local to regional scale climate change, *J. Geophys. Res.*, 98, 7289–7316, 1993.
- Hou, Y.-T., Cloud-radiation-dynamics interaction, Ph.D. dissertation, 209 pp., Univ. of Md., College Park, 1990.
- Kinter, J. L., J. Shukla, L. Marx, and E. K. Schneider, A simulation of the winter and summer circulations with the NMC global circulation model, *J. Atmos. Sci.*, 45, 2486–2522, 1988.
- Kitoh, A., K. Yamakazi, and T. Tokioka, Influence of soil moisture and surface albedo changes over the African tropical rain forest on summer climate investigated with the MRI-GCM-I, *J. Meteorol. Soc. Jpn.*, 66, 65–86, 1988.
- Kuo, H. L., On the formation and intensification of tropical cyclones through latent heat release by cumulus convection, *J. Atmos. Sci.*, 22, 40–63, 1965.
- Lacis, A. A., and J. E. Hansen, A parameterization for the absorption of solar radiation in the Earth's atmosphere, *J. Atmos. Sci.*, 31, 118–133, 1974.
- Laval, K., and L. Picon, Effect of a change of the surface albedo of the Sahel on climate, *J. Atmos. Sci.*, 43, 2418–2429, 1986.
- Lean, J., and D. A. Warrilow, Simulation of the regional climatic impact of Amazon deforestation, *Nature*, 342, 411–413, 1989.
- Mellor, G. L., and T. Yamada, Development of a turbulence closure model for geophysical fluid problems, *Rev. Geophys.*, 20, 851–875, 1982.
- Miyakoda, K., and J. Sirutis, *Manual of the E-Physics*, Princeton University Press, Princeton, N. J. 1986.
- Mylne, M. F., and P. R. Rowntree, Modelling the effects of albedo change associated with tropical deforestation, *Clim. Change*, 21, 317–344, 1992.
- Nobre, C. A., P. J. Sellers, and J. Shukla, Amazonian deforestation and regional climate change, *J. Clim.*, 4, 957–988, 1991.
- Panofsky, H. A., and G. W. Brier, *Some Applications of Statistics to Meteorology*, 244 pp., Pennsylvania State University, University Park, 1958.
- Pielke, R. A., G. A. Dalu, J. S. Snook, T. J. Lee, and T. G. F. Kittel, Nonlinear influence of mesoscale land use on weather and climate, *J. Clim.*, 4, 1053–1069, 1991.
- Polcher, J., and K. Laval, A statistical study of the regional impact of deforestation on climate using the LMD GCM, *IAHS Publ.* 214, 113–118, 1993.
- Sela, J. G., Spectral modeling at the National Meteorological Center, *Mon. Weather Rev.*, 108, 1279–1292, 1980.
- Sellers, P. J., Y. Mintz, Y. C. Sud, and A. Dalcher, A simple biosphere model (SiB) for use within general circulation models, *J. Atmos. Sci.*, 43, 505–531, 1986.
- Slutz, R. J., S. J. Lubker, J. D. Hiscox, S. D. Woodruff, R. L. Jenne, D. H. Joseph, P. M. Streurer, and J. D. Elms, *COADS: Comprehensive Ocean-Atmosphere Data Set, Release 1*, 262 pp., Climate Research Program, Environmental Research Laboratories, Boulder, Colo., 1985.
- Stephens, G. L., and T. J. Greenwald, The Earth's radiation budget and its relation to atmospheric hydrology, 1, Observations of the clear sky greenhouse effect, *J. Geophys. Res.*, 96, 15,311–15,324, 1991.
- Sud, Y. C., and M. J. Fennessy, An observational-data based evapotranspiration function for general circulation models, *Atmos. Ocean*, 20, 301–316, 1982.
- Sud, Y. C., and A. Molod, A GCM simulation study of the influence of Saharan evapotranspiration and surface-albedo anomalies on July circulation and rainfall, *Mon. Weather Rev.*, 116, 2388–2400, 1988.
- Sud, Y. C., W. C. Chao, and G. K. Walker, Dependence of rainfall on vegetation: Theoretical considerations, simulation experiments, observations, and inferences from simulated atmospheric soundings, *J. Arid Environ.*, 25, 5–18, 1993.
- Tiedke, M., The effect of penetrative cumulus convection on the large scale flow in a general circulation model, *Beitr. Phys. Atmos.*, 57, 216–239, 1984.
- Willmott, C. J., C. M. Rowe, and Y. Mintz, Climatology of the terrestrial seasonal water cycle, *J. Climatol.*, 5, 589–606, 1985.
- Xue, Y., P. J. Sellers, J. L. Kinter, and J. Shukla, A simplified biosphere model for global climate studies, *J. Clim.*, 4, 345–364, 1991.

P. A. Dirmeyer and J. Shukla, Center for Ocean-Land-Atmosphere Studies, 4041 Powder Mill Road, Suite 302, Calverton, MD 20705-3106.

(Received December 1, 1993; revised May 4, 1994; accepted May 13, 1994.)